J Solid State Electrochem (2004) 8: 592–598
DOI 10.1007/s10008-003-0493-6

ORIGINAL PAPER

Bernard A. Boukamp · Matthijs W. den Otter
Henny J. M. Bouwmeester

Transport processes in mixed conducting oxides: combining time domain experiments and frequency domain analysis

Received: 11 June 2003 / Accepted: 29 September 2003 / Published online: 21 February 2004

Abstract The conductivity relaxation (CR) method is often used for measuring the surface transfer rate, K_{tr}, and the bulk diffusion coefficient, $\tilde{D}$, for oxygen transport in mixed conducting oxides (MIECs). The time domain analysis of the obtained CR response is rather complex and is based on 'ideal' behaviour for the diffusion process. It is quite favourable to perform the data analysis in the frequency domain, where 'non-ideal' responses are easily recognised. Besides, frequency domain analysis (impedance spectroscopy) can yield reliable parameter estimates. Using a discrete Fourier-transform procedure, the time domain responses can be transformed to a frequency domain impedance-type expression. This approach can be applied to any system for which a driving force and a resulting flux can be defined.

Keywords Conductivity relaxation · Mixed ionic–electronic conduction · Oxygen diffusion · Fourier transform · Impedance analysis

Introduction

Mixed (electronic and oxygen ion) conducting oxides (MIECs) are being considered for potential applications such as SOFC cathodes and anodes, electrodes for oxygen pumps and as catalytically active membranes for membrane reactors. In all these processes three key parameters are essential for describing the electrochemical transport properties: (i) the electronic conductivity, (ii) the ionic conductivity or oxygen diffusivity and (iii) the surface exchange rate of oxygen, i.e. the rate at which ambient oxygen is transferred to a surface lattice site and vice versa.

The electronic conductivity is the simplest parameter to be measured; at least, when the electronic conductivity is significantly larger than the ionic conductivity, which is generally the case for the materials of interest. When the ionic conductivity is of the order of the electronic conductivity, or not more than about a factor 100 smaller, the two can be separated from simple two-electrode impedance measurements using ionically blocking electrodes. But one has to be aware of redox contributions in the electrode interface region, due to ac voltage-induced valence changes. Jamnik and Maier have recently presented a thorough analysis of the possible cases [1].

In cases where the ionic conductivity is significantly smaller than the electronic conductivity, direct electrical measurements can no longer be applied. One method to overcome this is by using an electrochemical cell with a closed fixed volume in which the MIEC is placed; see e.g. [2, 3, 4]. Using a special cell geometry it is also possible to use impedance spectroscopy for determination of the diffusion and transfer rates [5, 6]. These methods are, however, restricted in temperature range due to inherent limitations set forth by the glass seals.

A quite different approach is the ^{18}O-exchange technique [7]. Using secondary-ion mass spectroscopy (SIMS) the oxygen isotope diffusion profile is measured. Curve fitting yields the tracer diffusion coefficient and surface exchange rate. The method is generally very accurate, but also very costly and time consuming. An added advantage of this technique is that the influence of enhanced grain boundary diffusion can easily be detected [8].

The recently developed conductivity relaxation (CR) measurement technique [9] lacks the sealing restrictions and is relatively simple in the experimental setup. The useful temperature (and pO_2) range is mainly restricted by the response time of the sample. Hence, this method has become quite popular for the study of the oxygen transport process in the ferrite- and cobaltate-based

Presented at the OSSEP Workshop "Ionic and Mixed Conductors: Methods and Processes", Aveiro, Portugal, 10–12 April 2003

B. A. Boukamp (✉) · M. W. den Otter · H. J. M. Bouwmeester
Laboratory for Inorganic Materials Science,
Department of Science and Technology,
University of Twente, P.O. Box 217,
7500 AE Enschede, The Netherlands
E-mail: b.a.boukamp@utwente.nl

perovskite ceramics [10, 11, 12, 13, 14, 15] and related oxides [16, 17, 18, 19, 20].

In this method, the time-dependent change in the electronic conductivity is measured after a stepwise change in the ambient oxygen partial pressure. For small pO_2 steps it may be assumed that, through local equilibrium of the defect mechanisms, the electronic conductivity changes linearly with the oxygen (vacancy) concentration. Hence, through this indirect method the oxygen diffusion and surface transfer rate can be obtained. Although the basic transport and transfer equations [21] and boundary conditions are quite simple, the time domain solution for the conductivity relaxation is a rather complex infinite summation of non-analytical terms. Using carefully selected conditions and restrictions the measured responses can be modelled using a spreadsheet-type program or dedicated software. Caution, however, must be applied in the interpretation of the results [22], as will be presented in this contribution. Using Fourier transformation, the CR response data can be transferred to the frequency domain resulting in an impedance-type expression [13]. It will be shown that frequency domain analysis has a clear advantage over time domain analysis, as it presents a visual picture of the limitations of the CR method.

Conductivity relaxation

The transport equations are schematically presented in Fig. 1. A further derivation can be found in the literature and the contribution by Bouwmeester et al. in this issue [23]. For simplicity, we will consider only one-dimensional diffusion, i.e. the assumption of a thin slab with the x-dimension (thickness) much smaller than the other dimensions. Solutions for two-dimensional diffusion (cylindrical or square/rectangular [9]) are available, but will not be considered here. The relative change in the oxygen concentration in the MIEC, $\bar{c}_{\mathrm{step}}(x,t)$, upon a stepwise change in the oxygen partial pressure is given by [21]:

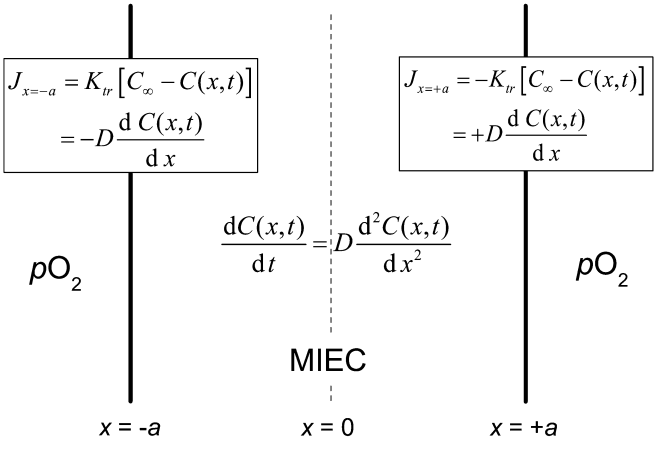

Fig. 1 Schematic representation of the oxygen transfer and diffusion process in a thin slab of thickness $2a$

$$\bar{c}_{\mathrm{step}}(x,t) = \frac{c_{\mathrm{step}}(x,t) - c_0}{c_\infty - c_0} = 1 - \sum_{n=1}^{\infty} \frac{2L_\alpha \cos(\alpha_n x/a)}{(\alpha_n^2 + L_\alpha^2 + L_\alpha)\cos(\alpha_n)} \exp\left(-\frac{t}{\tau_n}\right) \tag{1}$$

with:

$$\tau_n = \frac{a^2}{\tilde{D}\cdot\alpha_n^2} \quad \text{and} \quad L_\alpha = \frac{a\cdot K_{\mathrm{tr}}}{\tilde{D}} = \frac{a}{L_{\mathrm{c}}} \tag{2}$$

The sample thickness is given by $2a$, K_{tr} is the surface reaction rate and $\tilde{D}$ is the chemical diffusion constant. The equilibrium concentrations at $t=0$ and for $t\to\infty$ are presented by c_0 and c_∞. The ratio $\tilde{D}/K_{\mathrm{tr}}$ is known as the 'critical length' parameter, L_{c}, i.e. the sample thickness for which diffusion and surface transfer both determine the transport rate. When L_{c} is much larger than the half thickness a, the transport rate will be limited by surface exchange. For L_{c} values much smaller than the half sample thickness, diffusion limitation will dominate. The use of Eq. 1 requires finding the roots of the well-known expression:

$$\alpha_n \tan\alpha_n = L_\alpha \tag{3}$$

A simple, fast and accurate method for evaluation of Eq. 3 has recently been presented by den Otter et al. [24].

It is assumed that, for relatively small steps in the oxygen partial pressure, the electronic conductivity changes linearly with the oxygen ion concentration. Integrating Eq. 1 over the sample thickness yields the time domain expression for the *relative* change in the electronic conductivity, $\bar{\sigma}_{\mathrm{step}}$:

$$\bar{\sigma}_{\mathrm{step}} = \frac{\sigma(t) - \sigma_0}{\sigma_\infty - \sigma_0} = 1 - \sum_{n=1}^{\infty} A_n \cdot \exp\left(-\frac{t}{\tau_n}\right) \tag{4}$$

$\bar{\sigma}_{\mathrm{step}}$ evolves from 0 at $t=0$, to 1 for infinite time. The pre-exponential terms A_n are given by:

$$A_n = \frac{2L_\alpha^2}{\alpha_n^2(\alpha_n^2 + L_\alpha^2 + L_\alpha)} \tag{5}$$

The magnitude of the $L_\alpha$parameter, as defined in Eq. 3, is crucial for the determination of both $\tilde{D}$ and K_{tr} from a single relaxation curve [22]. This is clearly demonstrated by considering values for L_α that are much smaller, or much larger than 1. For $L_\alpha < 0.03$ Eq. 3 can be approximated by:

$$L_\alpha = \alpha_1 \tan\alpha_1 \approx \alpha_1^2 \tag{6}$$

Inserting this in the expression for τ_n, Eq. 2, results in a relation *independent* of $\tilde{D}$:

$$\tau_1 = \frac{a^2}{\tilde{D}\alpha_1^2} = \frac{a}{K_{\mathrm{tr}}} \tag{7}$$

The higher order roots of Eq. 6 can then be expressed as:

$$\alpha_n = \frac{L_\alpha}{n\pi} + n\pi \approx n\pi \tag{8}$$

Hence, the higher order time constants are approximated by:

$$\tau_n = \frac{a^2}{\tilde{D}\alpha_n^2} \approx \frac{a}{K_{\mathrm{tr}}} \cdot \frac{L_\alpha}{n^2\pi^2} \tag{9}$$

From Eq. 9 it is obvious that these time constants can be ignored, as they will appear at much shorter times thanτ_1, see Fig. 2. The magnitude of A_n terms will also decrease rapidly, as can be seen from Fig. 3.

When L_α is much larger than 1, e.g. $L_\alpha > 30$, the roots can be approximated by $\alpha_n \approx {}^1\!/_2\pi(2n-1)$.Thus, the time constants can be expressed as:

$$\tau_n = \frac{4a^2}{\tilde{D}\pi^2(2n-1)^2} \tag{10}$$

The ratios between pre-exponential terms, A_n, become the same as the ratios between the time constants, see Figs. 2 and 3:

$$A_1 : A_2 : A_3 : A_n = \tau_1 : \tau_2 : \tau_3 : \tau_n = 1 : \frac{1}{9} : \frac{1}{25} : \frac{1}{(2n-1)^2} \tag{11}$$

The first pre-exponential term, A_1, is equal to $8/\pi^2$, hence neither the pre-exponential terms nor the time constants contain information on K_{tr}. Thus in this regime it is not possible to determine K_{tr} from the conductivity relaxation curve. Figure 4 presents the simulated CR curves for a fixed$\tau_1 = 100$ s and three values of L_α: 0.03, 1 and 30. The curves with $L_\alpha = 0.03$ and $L_\alpha = 1$ are almost indistinguishable. Furthermore, from these curves it is not possible to guess in which regime the CR responses fall. The second-and third-order time constants and the related amplitudes, A_i, are essential for determining both $\tilde{D}$and K_{tr}. Unfortunately these parameters must be determined from the onset of the CR response curve, which generally is to some degree distorted by experimental influences. Further down this will be illustrated by the 'reactor flush time' problem.

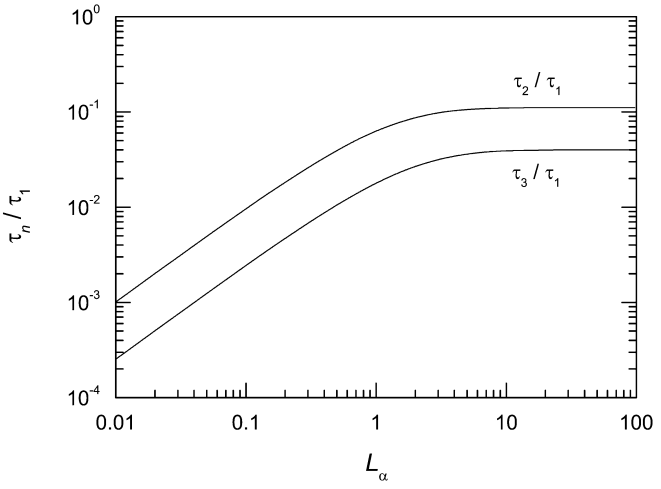

Fig. 2 Relative value of the higher order time constants with respect to τ_1 as function of L_α. For $L_\alpha > 30$ the ratios become constant (1/9, 1/25, ...). For $L_\alpha < 0.03$ the higher order time constants become negligible

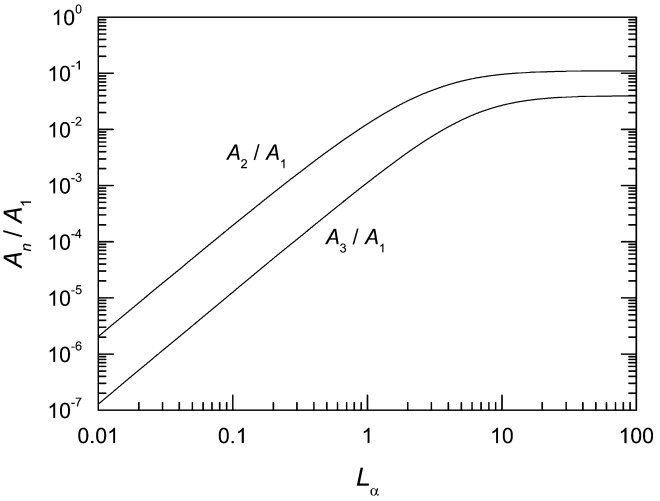

Fig. 3 Relative value of the higher order pre-exponential terms, A_n/A_1, as function of L_α. For $L_\alpha > 30$ these ratios also become constant (1/9, 1/25, ... cf. Fig. 2). For $L_\alpha < 0.03$ the higher order terms decrease rapidly, falling below the experimental noise level

Frequency domain analysis

The clear advantage of frequency domain analysis (i.e. impedance spectroscopy) is that the solution of the set of fundamental equations and boundary conditions generally has an analytical expression in the Laplace plane. Replacing the Laplace variable $s$by $j\omega$ directly leads to a frequency-dependent impedance-type expression. It is easy to show that the impedance, related to the oxygen flux through the interface and the partial pressure as driving force, results in the following expression:

$$Z(\omega) = \frac{L\{\Delta P_{\mathrm{O}_2}(t)\}}{L\{J(t)|_{x=\pm a}\}} = R_{\mathrm{tr}} + \frac{Z_0}{\sqrt{j\omega\tilde{D}}} \coth a\sqrt{\frac{j\omega}{\tilde{D}}} \tag{12}$$

This type of impedance is well known for electrochemical insertion electrodes. Measurements do not have to be obtained in the frequency domain, which in our case would require a frequency-adjustable oscillating oxygen partial pressure. Time domain data can be transformed to the frequency domain by Fourier transforms:

$$Z(\omega) = \frac{\overline{V(\omega)}}{\overline{J(\omega)}} = \frac{\int_0^\infty V(t) \cdot e^{-j\omega t}\mathrm{d}t}{\int_0^\infty J(t) \cdot e^{-j\omega t}\mathrm{d}t} \tag{13}$$

Here $V(t)$ and $J(t)$ represent the time domain driving force and flux. The CR measurements do not provide direct access to the oxygen flux, but a derived quantity $\sigma_{\mathrm{rel}}(t)$ is obtained in Eq. 4. Ten Elshof et al. [13] have

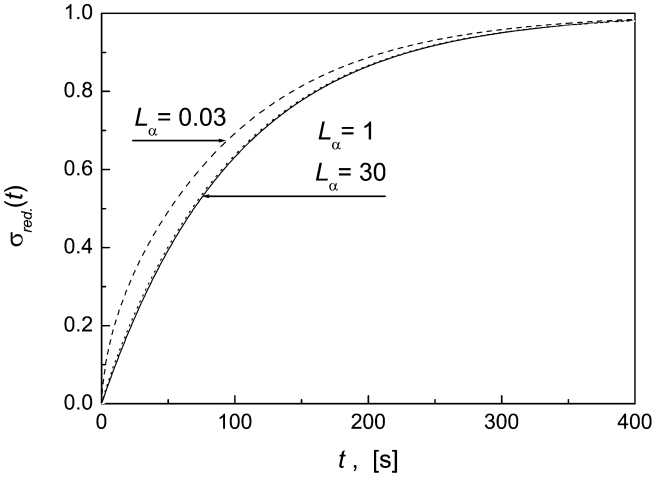

Fig. 4 Comparison of conductivity relaxation curves with $\tau_1 = 100$ s (*all*) and $L_\alpha = 0.03$, 1 or 30. The curves for $L_\alpha = 1$ (*dots*) and $L_\alpha = 30$ (*continuous line*) almost coincide

derived a modified impedance expression using the time domain CR response. The implicitly assumed step change in oxygen partial pressure has a simple Fourier transform, $\overline{V(\omega)} = \Delta P_{O_2}/j\omega$.The resulting impedance expression, which only contains the parameters a, $\tilde{D}$and K_{tr}, has the dimension of complex time:

$$Z_{CR}(\omega) = \frac{1}{\omega^2 \cdot \overline{\sigma_{rel}(\omega)}} = \frac{a}{K_{tr}} + \frac{a}{\sqrt{j\omega\tilde{D}}} \coth a\sqrt{\frac{j\omega}{\tilde{D}}} \qquad (14)$$

where $\overline{\sigma_{rel}(\omega)}$ represents the Fourier transform of the CR response (see below). The right-hand side of Eq. 14 has interesting features, the imaginary part of the low-frequency tail is equal to the inverse angular frequency, $Z_{im} = 1/\omega$. The changeover from the pure capacitive behaviour to the Warburg-type diffusion (45° slope) determines the value of $a/\tilde{D}$. When this changeover is not visible, the value of $\tilde{D}$ cannot be obtained from the measurement. On the other hand, if the extrapolation to high frequencies goes through the origin, then K_{tr} cannot be obtained from the measurement. This is clearly demonstrated in Fig. 5. From left to right the value of L_α is changed from $L_\alpha = 0.03$ (surface limitation) to $L_\alpha = 1$ and $L_\alpha = 30$ (diffusion limitation).

Fourier transform

Although the Fourier transformation (Eq. 13) is a quite simple expression, the actual transform is complicated by the discrete set of data and the limited time range. The integration can be approximated by a summation, for which several strategies are available [25]. A simple and fast summation is obtained by linear interpolation, $X_t = at + b$, between two successive data points, X_{i-1} and X_i:

$$\begin{aligned}\bar{X}(\omega) = \sum_{i=1}^{N} \Bigg[& X_i \sin\omega t_i - X_{i-1}\sin\omega t_{i-1} \\ & + \frac{a}{\omega}(\cos\omega t_i - \cos\omega t_{i-1})\Bigg]\omega^{-1} + \\ & - j\sum_{i=1}^{N}\Bigg[X_i\cos\omega t_i - X_{i-1}\cos\omega t_{i-1} \\ & - \frac{a}{\omega}(\sin\omega t_i - \sin\omega t_{i-1})\Bigg]\omega^{-1} \end{aligned} \qquad (15)$$

This method has been employed for the Fourier transformation of the data in Fig. 4 to obtain the impedance representations in Fig. 5. An important point is the finite time range of the data. Extrapolation to infinite time is essential for obtaining a useful Fourier transform. For the CR data this can be accomplished by modelling the end region of the data with an exponential function:

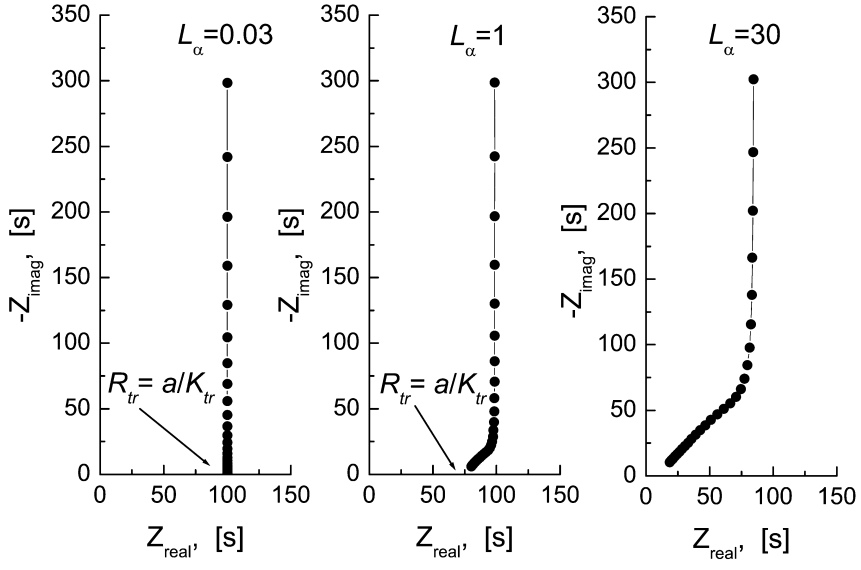

Fig. 5 The three impedance diagrams, transformed from CR simulations for different values of L_α, show clearly the exchange-limited (*left*) and the diffusion-limited (*right*) regimes. The frequency range is 534 μHz to 0.811 Hz. From the centre impedance both K_{tr} and $\tilde{D}$ can be obtained

$$X(t) = X_0 + X_1 e^{-t/\tau} \tag{16}$$

The Fourier transform from t_N to $t = \infty$ is then given by:

$$\overline{X(\omega)}\Big|_{t_N}^{\infty} = -\frac{X_0}{\omega}[\sin\omega t_N + \cos\omega t_N] + \\ + X_1 \cdot e^{-\frac{t_N}{\tau}}\left\{\frac{\tau^{-1}\cos\omega t_N - \omega\sin\omega t_N}{\omega^2+\tau^{-2}} + j\frac{\omega\cos\omega t_N + \tau^{-1}\sin\omega t_N}{\omega^2+\tau^{-2}}\right\} \tag{17}$$

This is especially essential when the long time tail has not yet reached a constant value, otherwise the first part of Eq. 17 with the X_0 term will suffice. This simplified method has been used to obtain the Fourier transformed impedance data of Figs. 5, 6 and 8. As an example the Fourier transform of a real CR response is presented in Fig. 6. The results for K_{tr} and $\tilde{D}$, obtained from both the time and frequency domain analysis, are presented in Table 1.

Flush time correction

In the CR experiments, it is generally assumed that the oxygen partial pressure change is instantaneous (step response). For samples with a slow response, i.e. low values for K_{tr} and $\tilde{D}$, this is adequate. One should realise, however, that changing the oxygen partial pressure in the volume of the measurement cell takes time. The simplest way of modelling this oxygen transient is by assuming CISTR (*continuous ideally stirred tank reactor*) conditions, in which case the time dependence of the partial pressure can be presented by:

$$p_{\mathrm{CISTR}}(t) = p_\infty + (p_0 - p_\infty)\cdot\exp\left(-\frac{t}{\tau_f}\right) \tag{18}$$

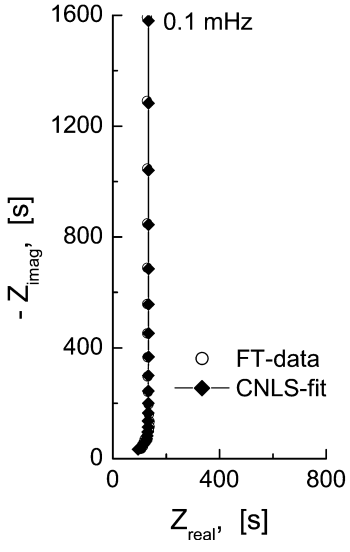

Fig. 6 Fourier transformed data set (*open circles*). Sample: $La_{0.7}Sr_{0.3}CoO_{3-\delta}$, with thickness 0.5 mm, $T = 728$ °C, pO_2 step 17 → 8 mbar. *Closed diamonds*: CNLS fit, using the 'Equivalent Circuit' software package. Results are presented in Table 1

Table 1 Results of data analysis in the time domain, Eq. <equationcite>4</equationcite>, and the frequency domain, Eq. <equationcite>14</equationcite>. Sample $La_{0.7}Sr_{0.3}CoO_{3-\delta}$, with thickness 0.5 mm, $T = 728$ °C, pO_2 step: 17 mbar → 8 mbar. The error estimate of the CNLS- fit [26] is based on the 67% confidence interval (1σ)

Parameter	FT-CNLS	1σ-rel. error	Time domain	Dimension
$R_{tr} = a/K_{tr}$	61.3	(4%)		[s]
K_{tr}	4.1×10^{-6}	(4%)	3.3×10^{-6}	$[m\cdot s^{-1}]$
$a/\sqrt{\tilde{D}}$	14.7	(2.5%)		$[s^{1/2}]$
$\tilde{D}$	2.8×10^{-10}	(4%)	3.2×10^{-10}	$[m^2\cdot s^{-1}]$

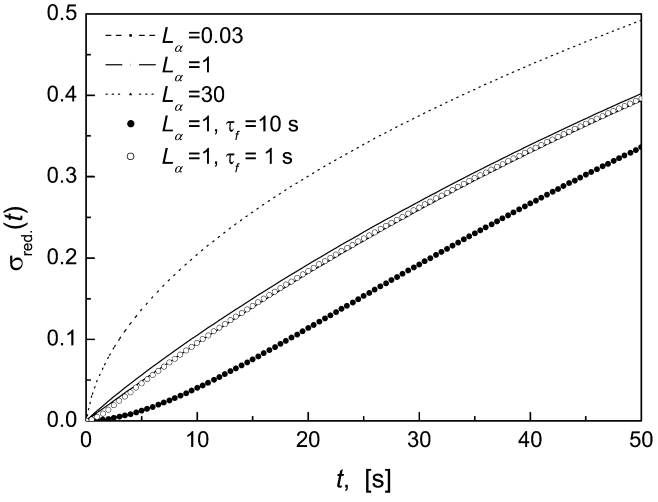

Fig. 7 Close-up of the first 50 s of the conductivity relaxation curve for three values of L_α (0.03, 1, 30) and for two flush time constants ($\tau_f = 1$, 10 s) for $L_\alpha = 1$. The figure clearly shows that the distinction between $L_\alpha = 1$, $L_\alpha = 30$ and $L_\alpha = 1$ combined with $\tau_f = 1$ s, is marginal

where τ_f is the time constant of the reactor and depends on the cell volume, V_{cell}, gas flow, $\Phi_{tot.}$, and temperature, T_{cell}. When the flow is measured at room temperature (T_0) the time constant becomes:

$$\tau_f = \frac{T_0}{T_{cell}}\cdot\frac{V_{cell}}{\Phi_{tot.}} \tag{19}$$

Combining the exponential change in the oxygen partial pressure with the basic transport equations for the relaxation process [22] leads to the convoluted response equation:

$$\bar{\sigma}_{\mathrm{CISTR}}(t) = 1 - \exp\left(-\frac{t}{\tau_f}\right) \\ -\sum_{n=1}^{\infty} A_n \frac{\tau_n}{\tau_n - \tau_f}\cdot\left[\exp\left(-\frac{t}{\tau_n}\right) - \exp\left(-\frac{t}{\tau_f}\right)\right] \tag{20}$$

The actual influence of the flush time problem is presented in Fig. 7, which has been restricted for clarity to the first 50 s. Again a basic time constant $\tau_1 = 100$ s and

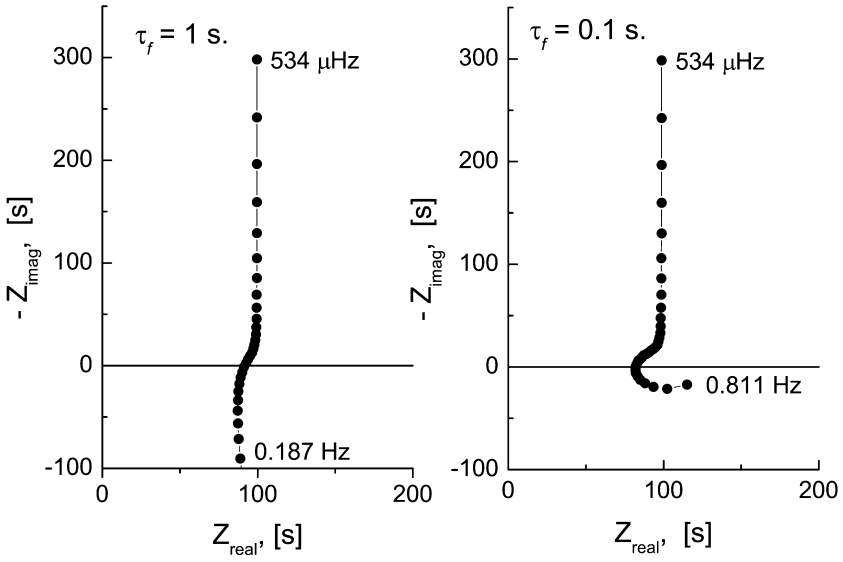

Fig. 8 Fourier transformed relaxation curves including the influence of a flush time delay. *Left*: flush time constant = 1 s. *Right*: flush time constant = 0.1 s. The first time constant of the conductivity relaxation curve is 100 s and $L_\alpha = 1$

$L_\alpha = 1$ is used (mixed limitation). The influence of a flush time constant of $\tau_f = 10$ s is clearly visible; it shifts the response curve to the right. The difference between the undisturbed curve and one with $\tau_f = 1$ s is much less apparent. If uncorrected, the analysis of the curve with $\tau_f = 1$ s will result in inaccurate values for $\tilde{D}$ and K_{tr} [26].

Again, a better approach is transformation to the frequency domain, presenting the response as an impedance. Transformations for flush times of $\tau_f = 1$ s and 0.1 s (with $\tau_1 = 100$ s and $L_\alpha = 1$) are presented in Fig. 8. The large high-frequency distortion (inductive loop) is only shown partly for the left-hand impedance graph ($\tau_f = 1$). However, even a small flush time constant of 0.1 s results in a distinct inductive loop. The Fourier transformed impedance is a convolution of the original impedance expression, Eq. 14, and the flush time function:

$$Z_{\text{app.}}(\omega) = (1 + j\omega\tau_f) \cdot Z_{CR}(\omega) \qquad (21)$$

Hence, transformation to the frequency domain presents a much more visual presentation of the limitations and complications of the CR experiments.

Conclusions

Fourier transformation of the CR response data presents clear insight into the limitations of the analysis. It can also easily provide error estimates for the obtained parameters, $\tilde{D}$and K_{tr}. Moreover, it can clearly indicate the negative influence of 'flushing problems', which are signified by a high-frequency inductive loop in the impedance plot. Also other distortions, e.g. due to the data acquisition system, will become evident in the frequency domain presentation.

The frequency domain analysis can equally well be applied to measurement of weight changes upon a stepwise change in the pO_2 [27, 28, 29]. In these types of microbalance setups with relatively large reactor volumes, the flush time could pose a significant problem, which can be recognized in the frequency domain.

This time domain measurement/frequency domain analysis can also be applied successfully to extend the low-frequency limit for impedance measurements down to the micro-Hertz level [30].

References

1. Jamnik J, Maier J (1999) J Electrochem Soc 146:4183
2. Lade K, Jacobsen T (1994) Solid State Ionics 72:218
3. Lankhorst MHR, Bouwmeester HJM (1997) J Electrochem Soc 144:1261
4. Diethelm S, Closset A, Nisancioglu K, Van herle J, McEvoy AJ (1999) J Electrochem Soc 146:2606
5. Nisancioglu K, Gür TM (1994) Solid State Ionics 72:199
6. Diethelm S, Closset A, Van herle J, McEvoy AJ, Nisancioglu K (2000) Solid State Ionics 135:613
7. Chater RJ, Carter S, Kilner JA, Steele BCH (1992) Solid State Ionics 53–56:859
8. Fielitz P, Borchardt G, Schmücker M, Schneider H (2003) Solid State Ionics 160:75
9. Yasuda I, Ishinuma M (1994) In: Ramanarayanan TA, Worrell WL, Tuller HL (eds) Proceedings of the 2nd international symposium on ionic and mixed conducting ceramics (Electrochemical Society proceedings series PV 1994-12). Electrochemical Society, Pennington, NJ, pp 209–221
10. Ma B, Balachandran U, Park J-H, Segre CU (1996) Solid State Ionics 83:65
11. ten Elshof JE, Lankhorst MHR, Bouwmeester HJM (1997) Solid State Ionics 99:15
12. Lane JA, Benson SJ, Waller D, Kilner JA (1999) Solid State Ionics 121:201
13. ten Elshof JE, Lankhorst MHR, Bouwmeester HJM (1997) J Electrochem Soc 144:1060
14. Lane JA, Kilner JA (2000) Solid State Ionics 136–137:997
15. Wang S, Verma A, Yang YL, Jacobson AJ, Abeles B (2001) Solid State Ionics 140:125
16. Song C-R, Yoo H-I (1999) Solid State Ionics 120:141
17. Song C-R, Yoo H-I (1999) Solid State Ionics 124:289
18. Rom I, Jantscher W, Sitte W (2000) Solid State Ionics 135:731
19. Kang S-H, Yoo H-I, Joung CY, Lee YW (2001) Solid State Ionics 140:257

20. Mauvy F, Bassat JM, Boehm E, Dordor P, Loup JP (2003) Solid State Ionics 158:395
21. Cranck J (1975) The mathematics of diffusion, 2nd edn. Clarendon, Oxford
22. den Otter MW, Bouwmeester HJM, Boukamp BA, Verweij H (2001) J Electrochem Soc 148:J1
23. Bouwmeester HJM, den Otter MW, Boukamp BA (2004) Oxygen transport in $La_{0.6}Sr_{0.4}Co_{1-y}Fe_yO_{3-\delta}$. J Solid State Electrochem (submitted)
24. den Otter MW, van der Haar LM, Bouwmeester HJM (2000) Solid State Ionics 134:259
25. Boukamp BA (to be published)
26. Boukamp BA (1986) Solid State Ionics 20:31
27. Katsuki M, Wang S, Yasumoto K, Dokiya M (2002) Solid State Ionics 154–155:589
28. Yashiro K, Onuma S, Kaimai A, Nigara Y, Kawada T, Mizusaki J, Kawamura K, Horita T, Yokokawa H (2002) Solid State Ionics 152–153:469
29. Ma B, Balachandran U (1997) Solid State Ionics 100:53
30. Boukamp BA (2004) Solid State Ionics (in press)